A measurement of double-polarization photoproduction on various nuclei.

The Real Gamma GDH Experiment on Nuclei (REGGEON)

A Letter of Intent to Jefferson Lab PAC 51

M. M. Dalton*‡, A. Deur*, C. D. Keith

Thomas Jefferson National Accelerator Facility, Newport News, VA 23606, USA

S. Širca*

University of Ljubljana, Ljubljana, Slovenia

* Spokesperson

‡ Contact

Abstract

We propose to measure the integrand of the Gerasimov-Drell-Hearn (GDH) sum rule on various light to medium sized nuclei in the energy range of 1.5–12 GeV in Hall D at Jefferson Lab. This would provide the first data on the GDH integrand on any nucleus heavier than ^{3}He. When combined with data having photon energies down to the pion production threshold to produce the full GDH integrand, it would constitute measurements of the modification of the anomalous magnetic moment of a nucleon in various nuclei. This will provide a new window into the modification of the nucleon in a nucleus. The experiment will also determine whether a polarized nucleon in a nucleus maintains its polarization when it is part of a short range correlation. The experiment will require polarized beam and a polarized target.

CONTENTS

I. EXECUTIVE SUMMARY

Main physics goals: The letter of intent deals with making novel measurements to study nucleon modifications within the nucleus using polarization observables.

Proposed measurement: The first goal is to measure the helicity-dependent part of the total photoproduction cross-section $\Delta\sigma$ on four light to medium sized polarized nuclei with polarized photons in the energy range of approximately 1.5–12 GeV as a novel probe of nucleon medium modifications.

The second goal is to measure $\mathbb{E}$, the beam–target double-polarisation observable in photoproduction from ^{7}Li, for a range of single meson production final states with a correlated nucleon pair. The dependence of this asymmetry on the nucleon relative momentum can be interpreted as a probe of the polarization of the nucleons in the correlated pair, which is predicted to be quenched as neutron-proton short range correlation (SRC) pairs form via tensor interaction. This would be the first direct study of high-momentum part of the nucleon distributions with polarization observables that we are aware of.

Specific requirements on detectors, targets, and beam: The experiment is proposed for Hall D at Jefferson Lab. It will require the same equipment as experiment E12-20-011 (approved at PAC 48, also known as Real Gamma GDH Experiment (REGGE) [1]), namely a circularly polarized photon beam and a longitudinally polarized target. The photon beam will have a flux less than the Gluex-II experiment (E12-13-003) and will be produced from a longitudinally polarized electron beam. In order to span the required range in photon energies, the experiment will run at two different CEBAF electron beam energies, nominally 4 and 12 GeV for this letter. Hall D is uniquely suited for such a measurement thanks to its high-resolution, high-efficiency photon tagger and its high-luminosity, large-solid-angle detector. The experiment will require 10 PAC weeks at the nominal CEBAF energy and another 4 PAC weeks at a lower beam energy in the range 3–4 GeV (nominally 4 GeV).

Related proposals: This experiment would use the same experimental setup and target apparatus as experiment E12-20-011. There, the convergence of the GDH integral at high energy and the validity of the GDH sum rule will be tested on both the proton and neutron. Experiment E12-14-001 will run in Hall B and measure the "spin-EMC" effect on ^{7}Li in the range $1 < Q^2 < 15\,\mathrm{GeV}^2$ and $0.06 < x < 0.8$.

II. INTRODUCTION

The understanding and description of the properties of nucleons bound in the nuclear medium is a fundamental problem of nuclear physics. Furthermore, such knowledge is critical for other physics programs which require a good understanding of the nuclear parton distribution functions, such as neutrino-nucleus scattering at FNAL, nucleus-nucleus scattering at RHIC or CERN, or electron-nucleus scattering at the future EIC.

Many properties of nucleons may be modified in the nuclear medium. Arguably, the most famous of these is the EMC effect, a suppression of the structure functions in the range $0.3 < x < 0.7$. This provides the strongest evidence that the nucleus cannot be described as a collection of bound pristine nucleons. It is interpreted as a modification of the partonic structure of the nucleon, rather than a bulk static property, so it is directly associated with the underlying QCD degrees of freedom. On the 40th anniversary of the initial observation of the EMC effect [2] there is still no complete and universally agreed-upon explanation for this suppression. Among the many explanations put forth, two main proposed mechanisms have emerged.

The first idea is that nucleons experience a modification due to a nuclear "mean field" that affects the internal quark distributions [3]. The modification depends on the nuclear density or binding experienced by a nucleon and therefore affects all nucleons similarly.

The second idea is that the modification is directly proportional to the extent to which the nucleon is off-shell, or moving at a high momentum [4, 5]. In this case the modification is an average over the majority of nearly-on-shell, slow-moving nucleons which are essentially unmodified, and a minority of highly-modified, far-off-shell, high-momentum nucleons that are within a short-range correlation (SRC).

New measurements are required in order to disentangle various possible explanations. Measurement of the spin and flavor dependence of the EMC effect along with measurements of other medium modification observables will provide new information important for developing a full understanding of the nucleon in the nuclear medium [6].

The spin structure functions are proposed as a way to differentiate between the mean-field and SRC explanations of the EMC effect. Mean-field models predict a large polarized EMC effect, while nucleons in SRCs, being expected to carry very little of the nuclear polarization, should show a very small effect [7, 8]. Experiment E12-14-001 [9], to measure the "spin-

EMC" effect on ^{7}Li in the ranges $1 < Q^2 < 15\,\mathrm{GeV}^2$ and $0.06 < x < 0.8$, has been approved to run in Hall B at JLab to measure this effect.

Flavor structure functions may also provide discriminating information. In mean-field models the u and d quarks may be modified differently in the nuclear medium, producing an isovector or flavor-dependent EMC effect. This occurs when the strong isovector forces in nuclei couple with different numbers of neutrons and protons in the nucleus, for example leading to u quarks that have a much larger EMC effect than the d quarks in ^{208}Pb [10]. SRCs are predominantly np pairs, which occur approximately 20 times more often that nn and pp pairs [11]. Since they are predominantly isoscalar, they cannot produce an isovector EMC effect.

We propose to take double polarization data on various light to medium sized nuclei (for example ^{7}Li, ^{13}C, ^{17}O and ^{19}F) with photons in the energy range of approximately 1.5–12 GeV. This range is achievable in Hall D using 2 different electron beam energies.

As described in Sec. III D there is strong reason to believe that there will be a significant modification of the helicity dependent total cross section in this region for a polarized nucleon in the nucleus. Combined with similar data from photons with energy from pion production threshold to 1.5 GeV, this would give the *integral* of the Gerasimov-Drell-Hearn (GDH) sum rule for a polarized nucleon in the nucleus. That integral is proportional to κ/M, the ratio of the anomalous magnetic moment to the mass of a nucleon. Measuring the modification of this quantity in a nucleus would be a unique new contribution to the general study of the medium modification of nuclei in the nuclear environment.

There is debate in the literature as to the size of any spin-EMC effect if the unpolarised EMC effect is driven by short range correlations (SRC). It is suggested in Ref [8] that since the tensor component of the nuclear force is dominant in creating the SRC pair, there is a depolarization of the nucleons in the pair and this must suppress any spin-dependent EMC effect. We propose a direct test of this depolarization hypothesis by measuring target spin asymmetries as a function of pair relative momentum, particularly as it exceeds the Fermi momentum. For this we will take a higher statistics data set on a single nucleus with the highest figure of merit (FOM). Table II gives some nucleus options with expected FOM values. Future R&D will determine what molecules produce the best polarization values and what those polarizations are and this may change the relative FOM of various species. Currently, ^{7}Li has the highest FOM.

The experiment is intended for Hall D. It is a logical continuation of E12-20-011 and apart from installing different target materials there will be no new equipment or special running conditions. It will require a circularly polarized photon beam (produced from a longitudinally polarized electron beam) with a flux less than the GlueX-II experiment E12-13-003. In order to span the required range in photon energies, the experiment will run at two different CEBAF electron beam energies. Hall D is uniquely suited for such a measurement thanks to its high-resolution, high-efficiency photon tagger and its high-luminosity, large-solid-angle detector.

The REGGE Experiment will test the convergence of the GDH integral at high energy and the numerical validity of the GDH sum rule will be tested on both the proton and neutron, to high precision. That data will give a baseline for measuring the modification of the nucleon spin properties in medium. The Hall D polarized target, developed for E12-20-011, will be used again for REGGEON. A major advantage of using a photon beam for studying polarized nuclear targets is its relatively minor effect on the target. Most molecules polarized using the dynamic nuclear polarization technique would loose significant polarization in an electron beam at a typical useful luminosity, making such measurements infeasible or more difficult. Running the experiment discussed in this LOI accompanying REGGE would maximize the efficiency.

While the experiment in this LOI proposes to study medium modifications at $Q^2 = 0$, there is a relationship between it and the spin-EMC measurement of experiment E12-14-001. The GDH sum is the $Q^2 \to 0$ limit of the generalized GDH sum which can be expressed as an integral over the spin structure function $g_1(x)$ at fixed Q^2:

$$I_{\mathrm{GDH}}(Q^2 \neq 0) = \frac{16\pi^2\alpha}{Q^2} \int g_1(x, Q^2) dx. \tag{1}$$

This relates the hadronic degrees of freedom at the real photon point to partonic degrees of freedom at high Q^2. A thorough understanding of the EMC effect would produce a model of the polarized structure functions such that the limit $Q^2 \to 0$ can be taken, integral over x performed, and compared to the data obtained here which then provide a strict constraint on the theory used to model the medium-modified spin structure function. This is an opportunity unique to this observable, as an analogous relationship to Eqn. (1) does not exist for the unpolarized case.

The measurements described here will add new data that are complementary to existing studies of medium modifications. As a novel approach to studying this topic, surprises are quite possible.

Notation: Throughout this document, a medium-modified quantity will be denoted by an asterisk, e.g. M^*.

III. INCLUSIVE MEASUREMENT

A. The Gerasimov-Drell-Hearn sum rule

The Gerasimov-Drell-Hearn (GDH) sum rule [12] is a general and fundamental relation that links the anomalous magnetic moment κ of a particle to its helicity-dependent photoproduction cross-section:

$$I \equiv \int_{\nu_0}^{\infty} \frac{\Delta\sigma(\nu)}{\nu}\,\mathrm{d}\nu = \frac{4\pi^2 S\alpha_{\mathrm{em}}\kappa^2}{M^2}, \tag{2}$$

where ν is the probing photon energy, S is the spin of the target particle, M is its mass, ν_0 is the minimum photon energy that can be absorbed by the target, α_{em} is the electromagnetic coupling constant, and $\Delta\sigma \equiv \sigma_P - \sigma_A$ is the difference in total photoproduction cross-sections ($\gamma A \to X$) for which the photon spin is parallel and anti-parallel to the target particle spin, respectively.

The sum rule is valid for any type of target particle: nucleons, nuclei, electrons, even photons. Equation (2) reveals that a non-zero anomalous magnetic moment, κ, is related to the excitation spectrum of the target and therefore its composite nature. The right-hand side of Eqn. (2) $I^N \approx 200\,\mu$b for the nucleon. The value of I generally decreases for increasing atomic mass of nuclei due to the M_A^{-2} dependence, and is listed for a range of nuclei in Table III. Very few nuclei have values comparable to or greater than the value for the nucleon.

1. *Anomalous Magnetic Moment*

The total magnetic moment $\vec{\mu}$ is related to the spin $\vec{S}$ of a particle [13]

$$\vec{\mu} = \frac{e}{M}(Q + \kappa)\vec{S}\,, \tag{3}$$

where eQ is the charge of the particle. The Dirac magnetic moment of a structureless particle is given by

$$\vec{\mu} = \frac{Qe}{M}\vec{S}\,, \tag{4}$$

but it is not clear whether a "point-like" magnetic moment can be unambiguously defined for particles with spin-$^3/_2$ or greater. In this work we naively apply Eqn. (4) to all nuclei—it is not relevant for our purposes whether this equation strictly applies since we are interested in studying the spin-½ constituents within any higher spin state nuclei.

For a nucleus of mass $M \approx AM_p$ and charge Ze, Eqn. (3) becomes

$$\vec{\mu} \approx \frac{e}{AM_p}(Z + \kappa)\vec{S} \tag{5}$$

or, in terms of the nuclear magneton, $\mu_N = {}^e/_{2M_p}$,

$$\kappa = \frac{A}{2S}\frac{\mu}{\mu_N} - Z\,. \tag{6}$$

This permits us to compute an "anomalous" magnetic moment for all stable nuclei with spin and therefore also the static sides of the GDH sum rule (RHS of Eqn. (2)), which are listed in Table III.

B. The GDH sum rule for a nucleon

The GDH sum rule on nucleons is reviewed in [14] and more recently in the REGGE proposal [1]. The existing data for the proton and neutron are shown in Fig. 1 and the "running" or cumulative integral in Fig. 2. Fig. 1 shows that the resonance regions are much more clearly visible in the helicity difference than in the helicity sum (total cross section). There is even the hint of a 4th resonance "bump" before the onset of the smooth Regge-type behaviour at high energy. It can be seen in Fig. 2 that the $\Delta(1232)$ dominates

the integral. Table I shows the strength of the integral that comes from each of the resonance regions as determined by integrating the experimental data with somewhat arbitrary energy boundaries. There is some cancellation but it is largely positive for both the proton and neutron.

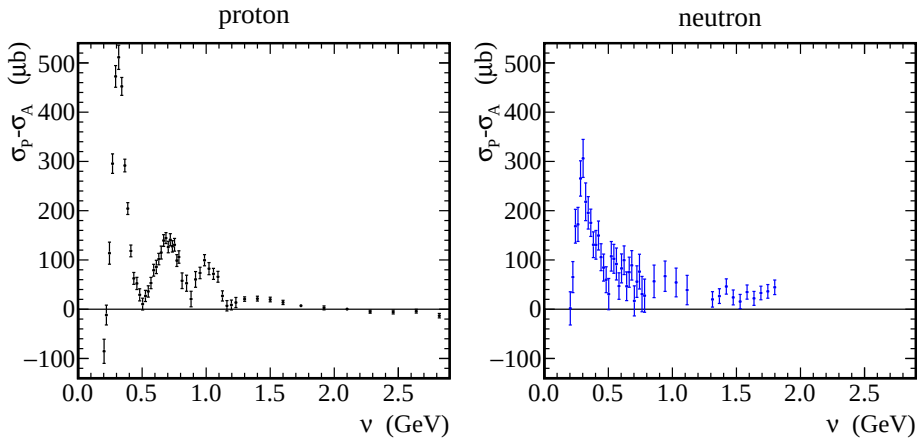

FIG. 1. World data of the spin-dependent cross-section difference $\Delta\sigma$ on the proton (left) and neutron (right). Data from various experiments are combined and rebinned.

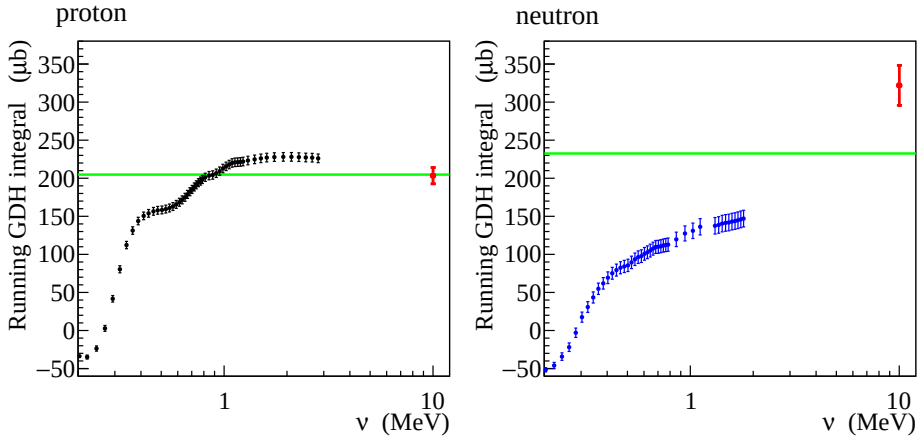

FIG. 2. The "Running" (cumulative integral) of the GDH integral for the proton (left) and neutron (right) using data from Fig. 1. The unmeasured contributions in $\nu_0 \leq \nu \leq 0.2\,\mathrm{GeV}$ are estimated to be $(-28.5 \pm 2)\,\mu$b and $\approx -41\,\mu$b, respectively, by the MAID2007 parameterization [15]. The green horizontal lines show the expected value of the GDH sum. The red points are the recent generalized GDH results from electroproduction extrapolated to $Q^2 = 0$ for the proton [16] and at $Q^2 = 0.035\,\mathrm{GeV}^2$ for the neutron [17].

TABLE I. Contributions to the GDH sum from the 3 resonance regions and the regions below and above the resonances. The values are given for the proton and neutron in cross section units and the percentage of the total integral. These values are obtained by performing the integral with somewhat arbitrary energy boundaries between the regions (statistical uncertainties only.)

	proton		neutron	
Energy region	I^p (μb)	I^p (%)	I^n (μb)	I^n (%)
Below Δ	-34.7 $\pm$ 2.2	-16.9 $\pm$ 1.1	-41 $\pm$ 2.6	-17.6 $\pm$ 1.1
Δ	190.9 $\pm$ 4.8	93.2 $\pm$ 2.3	137.0 $\pm$ 7.6	58.7 $\pm$ 3.2
2nd resonance	46.0 $\pm$ 1.7	22.5 $\pm$ 0.8	32.8 $\pm$ 4.2	14.0 $\pm$ 1.8
3rd resonance	17.5 $\pm$ 1.3	8.5 $\pm$ 0.6	15.8 $\pm$ 4.8	6.8 $\pm$ 2.1
Regge	-15.0 $\pm$ 5.9	-7.3 $\pm$ 2.9	88.9 $\pm$ 10.3	38.1 $\pm$ 4.4
Total	204.78	100	233.52	100

C. The GDH sum rule for a nucleus

A nucleus with a non-zero spin will necessarily have some non-zero value for the anomalous magnetic moment and the GDH integral. The nuclear magnetic moment arises from the unpaired spin of the constituent protons and neutrons. Due to the complexities of the nuclear force, the connection between the spin and the empirical magnetic moment of a nucleus is not easy to calculate.

The GDH integral on a nucleus will have contributions from the full photo-excitation spectrum from the lowest energy excitation, through the familiar "giant resonances", to excitation of or interaction with the nucleons themselves. An illustration of the spectrum versus photon energy can be seen for ^{56}Fe in Fig. 3. We show the unpolarized spectrum, rather than the polarized one pertaining to GDH, since the latter has not been measured on nuclei heavier than ^{3}He. The spectrum has been conceptually divided into the "photo-disintegration" region below the pion production threshold and the "photomeson" region above it. We assume that the region below is dominated by properties of the nucleus while the region above is dominated by properties of the nucleons. By studying the photomeson regime we are studying the medium-modified polarized-nucleon. Such a separation was performed in Ref. [18]. The unpolarized spectrum for ^{208}Pb can be seen in Fig. 4. Any coherent background from the nucleus that appears in the photomeson region is expected to be very small and can be partially measured, see Sec. V D 1.

As an illustration we consider a polarized nucleus where the polarization is carried by a single proton (as is approximately the case for ^{7}Li). In such a nucleus the contribution

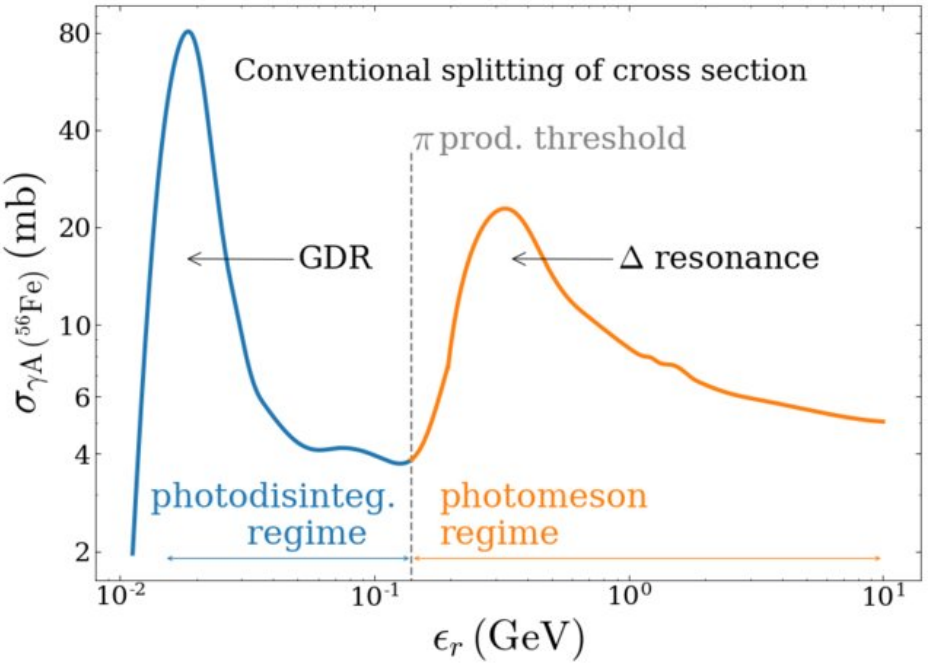

FIG. 3. The total unpolarized inelastic photonuclear cross section for ^{56}Fe, demonstrating the general shape for nuclei. It is separated into two regions at the photopion production threshold (≈ 140 MeV), the photodisintegration portion (in blue) and photomeson portion (in orange). For $\Delta\sigma$, the polarized cross-section difference pertaining to GDH, the photomeson regime is positive as in the figure, while the photodisintegration is expected to be negative for most nuclei. Figure from Ref. [19].

from the polarized proton to the GDH is expected to be on the order of $I^{p*} \approx 270\,\mu$b. This value is modified from the $I^p = 204.78\,\mu$b value of the free proton due to medium modification—the size is estimated in Sec. III D. The expected value of the GDH integral for ^{7}Li is $I^{^7\mathrm{Li}} = 83.4\,\mu$b as given in Table III and described in Sec III D.

Therefore, as a general rule, there must be a negative contribution coming from the low-ν photodisintegration region in order to cancel some of the contribution from the nucleon in the photomeson region. The ν^{-1} weighting means that the value of $\Delta\sigma(\nu)$ does not itself have to be large in the low-ν regime to produce a large cancellation.

We do not intend to extend the measurement below the meson production threshold since we are not aiming to test the GDH sum rule. Instead, we are interested in the possible modification of the integrand above the meson production threshold, which should resemble the spectra in Fig. 1 with Fermi broadening and medium modification effects such as an apparent change in $\Delta(1232)$ mass or an apparent change in the Regge intercept and slope that parameterize $\Delta\sigma$ for $E_\gamma \gtrsim 1.5\,$GeV.

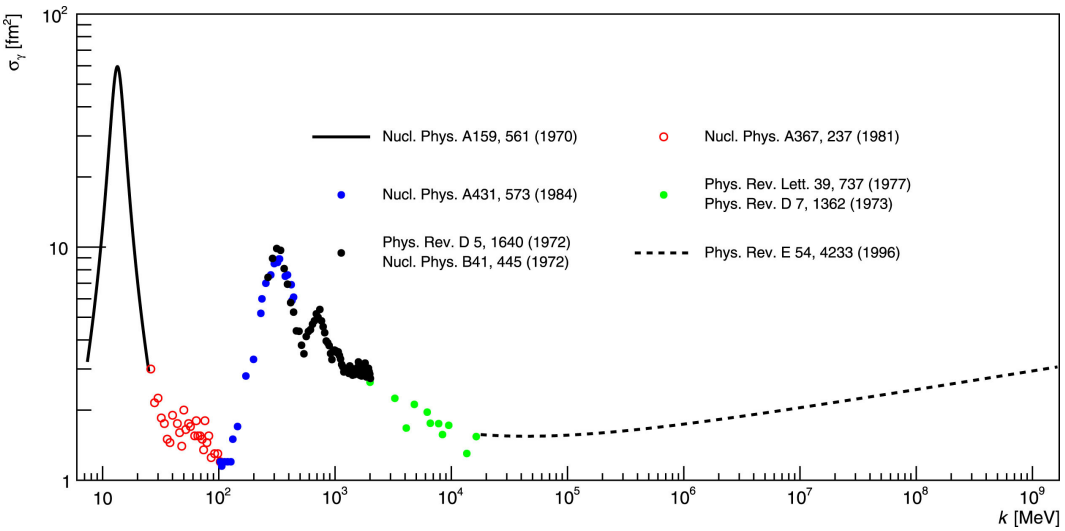

FIG. 4. The unpolarized cross section $\sigma(\gamma A \to A' + Xn(k))$ for ^{208}Pb. Various experiments and approaches are used in different energy ranges. Details in Ref. [20]. The figure serves simply to illustrate the excellent separation between photodisintegration and photomeson regions.

D. Modification of the nucleon GDH quantities in medium

A nucleon in the nuclear medium will be modified and this will lead to a modification of the nucleon GDH integral through Eqn. (2). Calculations [21, 22] of the medium modification affecting the GDH sum use the quark-meson coupling model (QMC) to predict a large enhancement in the GDH integral at density ρ_0 of ordinary nuclear matter. Here we perform a calculation of the size of the effect in more detail.

1. Right hand side, modification of mass and magnetic moment

The right hand side of Eqn. (2) is

$$I_{\rm RHS} \equiv \frac{4\pi^2 S \alpha_{\rm em} \kappa^2}{M^2} \, .$$

From a mean-field (QMC) calculation [23], the mass of the nucleon and of the $\Delta(1232)$ resonance both vary linearly with density (for $\rho \ll \rho_0$) as

$$\frac{M_N^*}{M_N} \approx \frac{M_\Delta^*}{M_\Delta} \approx \left(1 - 0.2 \frac{\rho}{\rho_0}\right) \, , \tag{7}$$

while the anomalous magnetic moment changes as

$$\frac{\kappa_N^*}{\kappa_N} \approx \left(1 + 0.1\frac{\rho}{\rho_0}\right) . \tag{8}$$

Note that only the anomalous part of the magnetic moment is modified in the nuclear medium; by definition the point-like part is unaffected. The anomalous part is also the part that appears in the GDH sum so that the modification will appear quadratically in the sum without the need to consider the point-like part. The low density relationships in Eqns. (7) and (8) were used in [21] to predict a factor of 2.1 increase in the integral in Eqn. (2). However, as the density approaches nuclear matter density the dependence flattens out, Fig. 5, and the linear approximation becomes an overestimate. At nuclear matter density

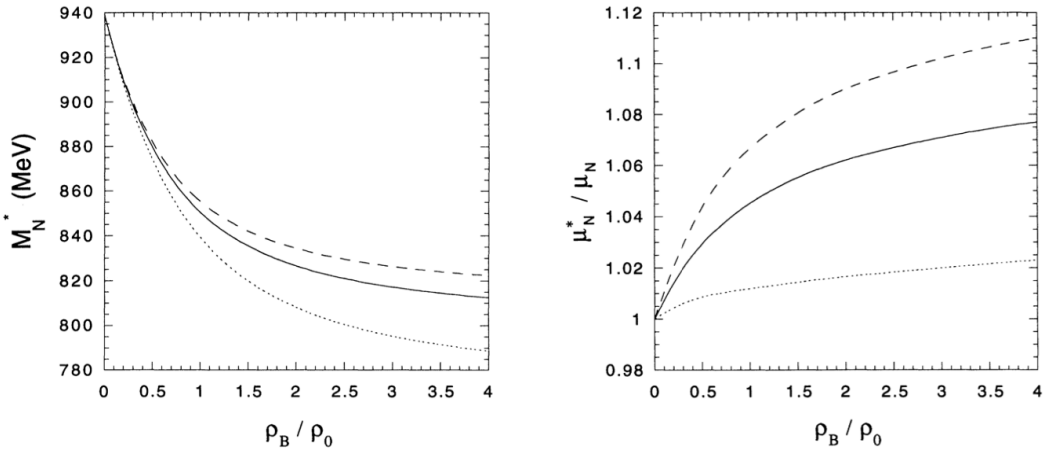

FIG. 5. Effective nucleon mass in symmetric nuclear matter (left) and the ratio of the magnetic moment of the proton in medium to that in free space (right) estimated in the QMC model with the nucleons modeled as MIT bags [24]. The dotted, solid, and dashed curves are for bag radii of 0.6, 0.8, and 1.0 fm, respectively. Figure from Ref. [24].

the values are, from Fig 5,

$$\begin{aligned} \frac{M_N^*(\rho_0)}{M_N} &= 90.4^{+0.5}_{-1.1}\,\%, \\ \frac{\kappa_N^*(\rho_0)}{\kappa_N} &= 104.5^{+2.3}_{-3.3}\,\%. \end{aligned} \tag{9}$$

The uncertainty was estimated by varying the bag size between 0.6 and 1.0 fm.

Therefore at nuclear matter density the effect on the ratio relevant to the GDH sum is

$$\frac{\left(\frac{\kappa^*(\rho_0)}{M_N^*(\rho_0)}\right)^2}{\left(\frac{\kappa}{M_N}\right)^2} = 133.6^{+4.4}_{-5.4}\,\% \tag{10}$$

with correlated uncertainties on κ^* and M_N^* due to the bag size partially cancelling. Importantly, even at densities below nuclear matter the effect would still be easily observable.

An updated publication [23], working with a "small density" approximation, gives $\frac{M_N^*(\rho_0)}{M_N} = 89\,\%$ and $\frac{\kappa_N^*(\rho_0)}{\kappa_N} = 107\,\%$ when extrapolated to nuclear matter density, and a ratio $\left(\frac{\kappa^*(\rho_0)}{M_N^*(\rho_0)}\right)^2 / \left(\frac{\kappa}{M_N}\right)^2 = 145\,\%$. This is likely an upper bound on the true value since the linear approximation found at small density does not apply at nuclear matter densities.

Using the value found in Eqn. (10) we estimate that the GDH integral values for the proton and the neutron at nuclear matter density are $I^{p^*} = 273 \pm 11\,\mu$b and $I^{n^*} = 312 \pm 13\,\mu$b at $\rho = \rho_0$, with uncertainties only from varying the bag size.

2. *Left hand side, modification of the helicity-dependent photoproduction cross-sections*

The left hand side of Eqn. (2) is

$$I_{\mathrm{LHS}} \equiv \int_{\nu_0}^{\infty} \frac{\Delta\sigma(\nu)}{\nu}\,\mathrm{d}\nu. \tag{11}$$

The dominant contribution to the GDH integral in both nucleons comes from the $\Delta(1232)$ resonance. This can be seen in Figs. 1 and 2 and is shown numerically in Table I. The proton and the neutron have contributions to I from the $\Delta(1232)$ of $\approx 90\%$ and $\approx 60\%$ respectively, with some cancellation from the regions below and above the resonances. In pion-nucleus scattering, the $\Delta(1232)$ peak shifts down in energy and gets broader as A increases [25]. This is also seen in the CQM model, Eqn. (7) from Ref. [24]. A shift of the resonance peak toward lower photon energies will enhance the $\Delta(1232)$ contribution to the nucleon GDH integral because of its integrand $\Delta\sigma/\nu$. The ν^{-1} dependence of the GDH integrand essentially translates into a M_Δ^{-1} dependence of the LHS of Eqn. (2). However, it is smaller than the $M_{\mathrm{nucleon}}^{-2}$ modification of the RHS. The effect of $\Delta(1232)$ modification can only be a fraction of the total spectrum modification required to agree with the right hand side.

Using M_N^* from Eqn. (9) and Table I, the $\Delta(1232)$ would naively explain less than 57% of the proton enhancement and less than 36% of the neutron enhancement. This argument is independent of the absolute size of the modification expected. Therefore there must be a sizable component that comes from the higher mass nucleon resonances and the Regge region.

In the second resonance region, the dominant $D_{13}(1520)$ appears to not change much in medium: inclusive single and multiple pion production data on the $D_{13}(1520)$ shows no peak motion or additional broadening beyond Fermi smearing [26]. The weaker $S_{11}(1535)$ is theoretically not expected to change much in medium [27]. The $S_{11}(1535)$ is a special case since it can be studied in medium through its emission of an η meson and serves here as additional confirmation for the $D_{13}(1520)$ and other resonances. Experiments in heavy-ion collisions [28] and η photoproduction from nuclei [29, 30] suggest little modification of the $S_{11}(1535)$ excitation in-medium (some evidence for the broadening of the S_{11} in nuclei was reported in [30]). This is confirmed in more recent data where no mass modification is observed [31, 32]. The main difference between the first and second resonance regions enters because the Δ has the 3 quarks in $(1s)^3$ and the second resonance region has the 3 quarks in $(1s)^2(1p)$ with the $1s$ wave-function more affected by medium structure than the $1p$.

The third resonance region and above together contribute almost nothing to the integral for the proton, due to cancellation, but a large 45 % to the integral for the neutron. This is consistent with the recent SAID estimate that for the neutron, the single pion production contributes about 56% to the GDH sum rule, while it amounts to 90% for the proton [33]. Since the modification in the first and second resonance regions cannot explain the full modification of the integral a large fraction of the modification to the GDH integral is expected in this region, which is covered by the existing GlueX tagger without modifications at a beam energy of about 4 GeV. Alternatively, it could be that the theoretical framework used to assess the nuclear modifications is incorrect. Thus, either there are large nuclear modifications in the Regge domain, or the available theoretical framework is defective, or both. In any case, this warrants an experimental investigation.

3. Regge Parameters

Regge theory predicts the cross-section at high energy to be described by the functional form

$$\sigma_P - \sigma_A = I c_1 s^{\alpha_{a_1}-1} + c_2 s^{\alpha_{f_1}-1}, \tag{12}$$

where the parameters must be determined from the data [34].

Regge theory suggests that at high ν, $\Delta\sigma(\nu) \propto (\nu + M/2)^{\alpha_0-1}$ [34], with α_0 a Regge intercept. For the isovector part, $\Delta\sigma^{p-n} \equiv \Delta\sigma^p - \Delta\sigma^n$, α_0 should be determined by the $a_1(1260)$ meson trajectory, which is still not well known. For the isoscalar $\Delta\sigma^{p+n} \equiv \Delta\sigma^p + \Delta\sigma^n$ part, α_0 should be given by the $f_1(1285)$, which is better known.

The REGGE Experiment will test Regge theory well into the region where it is expected to be applicable with expected uncertainties on the intercepts of $\Delta\alpha_{a_1} = \pm 0.007$ and $\Delta\alpha_{f_1} = \pm 0.029$. These expectations can be compared with the values $\alpha_{a_1} = \pm 0.23$ and $\alpha_{f_1} = \pm 0.22$ extracted from the ELSA data [14]. Given this high precision and the intention to obtain uncertainties on nuclei within a factor of 2 of those approved for proton and deuteron, this experiment should be sensitive to even small medium modifications of the Regge trajectories.

IV. EXCLUSIVE MEASUREMENT

Studies of the spin dependence of the EMC effect have been proposed as a new and fruitful direction to probe the underlying cause. Mean field models suggest an effect that is larger even that the original EMC effect [35–37]. On the other hand, it is less clear what the effect would be if SRCs dominantly cause the EMC effect. One concrete hypothesis is that nucleons in SRC are depolarized and would therefore show very little polarized EMC effect [8]. An experiment is planned at Jefferson Lab to measure the nuclear spin structure function to search for a spin EMC effect [9]. The interpretation of this experiment in terms of SRCs would require knowledge of the degree of polarization of nucleons in a pair.

We propose a direct and simple measurement of the degree of polarization of nucleons in an SRC and therefore test of this depolarization idea. If one can identify a target-asymmetry in the interaction of an electromagnetic probe and a polarized nucleon then one can use that asymmetry to measure the polarization as a function of the pair relative momentum, and see whether the nucleon remains polarized when in a SRC pair. The target-asymmetry could be

any difference in yield that depends on the target polarization direction. In more concrete terms, correlated pairs with relative momentum which is less than the Fermi momentum would not be in a SRC, while correlated pairs with higher relative momentum would be in a SRC. The asymmetry here is used only as an indicator of target polarization, and the unmodified value would be known from the REGGE Experiment. Observing that the target-asymmetry does not change from a finite value to zero as the relative-momentum exceeds Fermi momentum would be a clear rejection of the depolarization hypothesis in the SRC. Conversely, a reduction of the asymmetry would strongly suggest a depolarization effect.

The asymmetry the we consider here is $\mathbb{E}$, the beam–target double-polarisation observable in photoproduction. There are a number of potential reactions of interest here, we identify $\vec{A}(\vec{\gamma}, \rho^- pp)$ and $\vec{A}(\vec{\gamma}, \pi^- pp)$ as particularly promising. These have np pairs as the initial state, the single meson production of ρ or π from a nucleon has a large cross section, and the all-charged final state is relatively simple to detect. Other possibilities are $\vec{A}(\vec{\gamma}, \rho^0 pn)$ and $\vec{A}(\vec{\gamma}, \omega pn)$, $\vec{A}(\vec{\gamma}, \pi^0 pn)$, or $\vec{A}(\vec{\gamma}, \eta pn)$ which have smaller cross sections or lower detection efficiencies but are nevertheless viable. The reactions $\vec{A}(\vec{\gamma}, \rho^0 pp)$ and $\vec{A}(\vec{\gamma}, \omega pp)$ will allow a comparison with pp pairs in the initial state.

Values for $\mathbb{E}$ have not yet been measured in the energy range of interest for this experiment. Many of the final states of interest have been measured in the resonance region and display promisingly large asymmetries. In the resonance region they typically have a strong dependence on CM angle and W, consistent with contributions from multiple overlapping resonances with different spin and parity. This behavior is expected to become much smoother in the Regge region. The reaction $\vec{\gamma}\vec{p} \to \omega p$ was measured up to $W = 2.3\,\text{GeV}$ and shows an asymmetry of up to 40% at the highest masses [38]; $\vec{\gamma}\vec{p} \to \eta p$ was measured up to $W = 2.1\,\text{GeV}$ and shows an asymmetry of up to 70% at the highest masses [39]; $\vec{\gamma}\vec{p} \to \pi^0 p$ was measured up to $W = 2.3\,\text{GeV}$ and shows an asymmetry of up to 80% at the highest masses [40, 41]. Quark-hadron spin duality, verified on g_1^p and g_1^n [42, 43], argues that the asymmetries in the energy range of this proposal will be similarly large. The future REGGE Experiment [1] will measure them directly on p and D.

This asymmetry can then be measured again for nuclei where two correlated nucleons are emitted. In ^{7}Li the asymmetry should be diluted by a factor of 9, Table II. Therefore, the asymmetry is expected to be in the range of a few % to 10%.

A. Estimates based on the SRC/CT Experiment in Hall D

The SRC/CT Experiment [44] ran in Hall D on ^{2}H, ^{4}He and ^{12}C for 4, 10 and 14 days, respectively. While the analysis is ongoing, progress reports to Jefferson Lab management are very encouraging. Signal has been identified in the reaction $A(\gamma, \rho^- pp)$ for $-t > 1\,\mathrm{GeV}^2$, $-u > 1\,\mathrm{GeV}^2$ and $E_\gamma > 7\,\mathrm{GeV}$, for all targets. This is a clean SRC channel and would make a very attractive candidate if the asymmetry is large enough. Simple projections based on the preliminary analysis indicate that above the Fermi surface $k_{\mathrm{miss}} > 0.4\,\mathrm{GeV}$, ^{2}H and ^{12}C yielded about 350 of these events per day of running and ^{4}He yielded about 500 events per day.

A realistic product of beam and target polarizations, averaged over the beam energy range 7–12 GeV, is about 0.5. Given these numbers an asymmetry would be measured to approximately 2% with 10k events or about 4 PAC weeks of running. This is sufficient to observe a relatively large asymmetry diluted by ⅑ to 5σ. Significance would be increased by combining multiple final states.

With 16 PAC weeks of running or 40k events, an asymmetry would be measured to approximately 1%. This level of statistics would allow a significant study of smaller asymmetries without the need to combine final states. Alternatively, it would allow the k_{miss} dependence to be mapped. Dividing into 4 bins above the Fermi energy would give a 2% measurement in each bin.

V. EXPERIMENT

A. Beam

The beam was described in some detail in Ref. [1]. It will be produced by bremsstrahlung in the Hall D Tagger. Circularly polarized photons are produced from longitudinally polarized electrons and so the experiment would require an injector launch angle that gives longitudinal polarization in the hall. Ref [1] used a value $P_e = 80\%$ so that value is assumed here, since estimates are made using a simple scaling. Smaller P_e values would decrease the figure of merit. The experiment could run with the polarization direction not fully longitudinal but would require more time to achieve the same statistical power. The photons themselves get 100% of the longitudinal polarization at their maximum energy which de-

creases smoothly to zero at the minimum energy. The FOM is therefore favored at higher energy but Ref. [1] showed that the GDH measurement is viable at all tagged energies since the decrease in polarization is partially compensated for by the increase in flux at lower energies due to the $1/E$ bremsstrahlung spectrum.

B. Target

This experiment would use the same target apparatus, without modification, as was approved for REGGE [1]. In this system, target samples will be continuously polarized via dynamic nuclear polarization (DNP) inside the Hall D spectrometer at a temperature of 200–300 mK. The field strength of the Hall D solenoid varies from about 1.60 T to 1.65 T over the length of the proposed 10 cm long polarized sample. The target cryostat will therefore include internal superconducting coils to increase the field to 2.5 T and improve the homogeneity around the target sample to better than 300 ppm for optimal polarization. The planned photon flux of $\approx 10^8\,\mathrm{s}^{-1}$ will produce negligible target depolarization.

1. Choice of Nuclei

The choice of nuclei is driven by a number of potentially competing factors. Firstly, it is desirable that the polarization of the nucleus is carried by a single nucleon. This allows the interpretation of the signal as coming from a single nucleon with minimal corrections. Secondly, the nucleus should be large enough, and the polarized nucleon itself should be in a shell such that it will have a significant modification—this tends to favor larger nuclei. Thirdly, there is an intrinsic nuclear dilution due to the unpolarized nucleons such that the size of any asymmetry will drop linearly with the number of nucleons—this favors measurements on smaller nuclei. The asymmetry in a large nucleus is smaller and therefore requires more time to measure to the same precision.[1] It is a requirement is to know the effective polarisation of nucleons within the nucleus. This has been determined for $A \leq 12$ using the Green's Function Monte Carlo Method but recently other techniques such as Coupled Cluster, Self-Consistent Green's Function, In-Medium Similarity Renormalization Group have achieved high accuracy for nuclei even in to the calcium region with capability to use chiral

[1] Technically we are interested in the cross section difference but the total cross section limits the data collection rate so the asymmetry still governs the statistical precision.

NN and 3N interactions [45]. We expect that microscopic nuclear theory will continue to rapidly evolve.

Table III gives a list of stable nuclei with a known magnetic moment. In principle, any of those nuclear species can be polarized using the dynamic nuclear polarization (DNP) technique, but in practice DNP has been demonstrated in only a handful of nuclei. First, a suitable molecular compound with the species of interest must be identified. Second, the target sample must be homogeneously diluted with paramagnetic impurities at a concentration of about 10^{-4}. These are molecular radicals, ions, or other crystallographic defects featuring a single, unpaired electron. For target materials that are liquid at room temperature, the paramagnetic impurities may be introduced by dissolving a suitable free radical and freezing the solution into a glassy matrix. For room temperature solids, the impurities are created using ionizing radiation. The unpaired electrons are polarized at low temperature and high field; at the 300 mK and 2.5 T conditions of the polarized target, the polarization is greater than 99.9%. Microwave-induced spin flip transitions are then used to transfer this polarization to the nuclear spins.

Table II gives some examples of nuclear species and their possible parent molecules. Dynamic polarization has been demonstrated in each of these molecules, and the anticipated polarizations are given. In the case of ^{1}H, ^{2}H, and ^{7}Li, these are polarizations that have been achieved in other laboratories at ≈ 0.3 K and ≈ 2.5 T. High polarizations have also been demonstrated in ^{13}C and ^{19}F, albeit not at these exact conditions. The polarization of ^{17}O is estimated under the assumption that DNP will be as effective for this nucleus as it is for the other nuclei in the indicated compound, scaled by their respective magnetic moments. This is the so-called "Equal Spin Temperature" (EST) hypothesis for DNP, which has been found to be correct for numerous examples.

Research and development is needed to determine the the optimal FOM for various nucleus sizes. However, enough is already known to provide a good choice of nuclei for a pilot experiment such as the one discussed here, see Table II. Table II also demonstrates that the dilution from unpolarized nucleons is not significantly worse than for ^{1}H and ^{2}H since they too must be housed within an appropriate molecule for polarization.

TABLE II. The table gives information on ^{1}H and ^{2}H as approved for experiment REGGE [1], and for the nuclear species envisioned for use in this experiment. Included are expected polarization P, the polarized nucleon of study, the molecule used in the target, the dilution from unpolarized nucleons in the target molecule, the figure of merit from Eqn. (13), and the numbers of days required to equal the statistics for ^{1}H in REGGE for the regular (12 GeV) and low energy (4 GeV) runs.

	J^π	P	species	molecule	dilution F	FOM P^2F ($\times 10^{-3}$)	days 12 GeV	days 4 GeV
^{1}H	$1/2^+$	90%	$\vec{p}$	C_4H_9OH	$10/74 = 0.135$	110	7	4
^{2}H	1^+	80%	$\vec{n}$, $\vec{p}$	C_4D_9OD	$10/84 = 0.119$	76	10	6
^{7}Li	$3/2^-$	80%	$\vec{p}$	$^7Li^2H$	$1/9 = 0.111$	71	11	6
^{13}C	$1/2^-$	60%	$\vec{n}$	C_4D_9OD	$4/78 = 0.051$	4.6	42	24
^{17}O	$5/2^+$	80%	$\vec{n}$	$C_4D_9{}^{17}OD$	$1/75 = 0.013$	8.5	90	51
		80%	$\vec{n}$	$H_2{}^{17}O$	$1/19 = 0.053$	34	23	13
^{19}F	$1/2^+$	90%	$\vec{p}$	$^6Li^{19}F$	$1/25 = 0.040$	32	24	14
		80%	$\vec{p}$	$C_3H_2{}^{19}F_6O$	$6/168 = 0.036$	23	34	19

2. Inclusive Measurement

The neutron and proton have different GDH integrals and very different shapes of the GDH integrand, yet their modification in the nucleus is in many ways expected to be the same. For this reason it is important to study both nuclei and perform an isospin comparison. The proton is by far the more well studied nucleon and must be included. As argued previously, the neutron has a much larger $\Delta\sigma$ at high-ν than the proton, so the experiment proposed here is more sensitive to medium modifications for the neutron than the proton. A pair of measurements with modified neutron and modified proton would allow for an isospin comparison of the modification if the other differences between the two nuclei can be controlled for. As described in Sec. II, the general dependence of the size of medium modifications with A is unknown. Therefore, in order to more meaningfully compare the proton with the neutron we must also put a first order bound on an apparent dependence on average nucleon separation energy, "scaled nuclear density", or A. For this reason we propose to take data on 4 nuclear species, likely ^{7}Li, ^{13}C, ^{17}O and ^{19}F.

a. Lithium-7 Based on these considerations, a very strong candidate nucleus is ^{7}Li, which will be the subject of a $Q^2 > 1\,\mathrm{GeV}^2$ polarized EMC experiment at JLab [9]. ^{7}Li is expected to show a sizable EMC effect (somewhere between ^{3}He and ^{4}He if local density dominates the scaling). EMC data for ^{7}Li was recently obtained by E12-10-008 [46] and

results are expected soon. The spin is carried by a highly polarized proton with a relatively small dilution from unpolarized nucleons, it is amenable to precise microscopic calculations, and it has already been demonstrated to polarize well (COMPASS achieved a polarization of 90% at 0.3 K and 2.5 T [47, 48].) For many of the same reasons it should be included here and is the target that we will dedicate the most time to. This is primarily because of the strong complementary of the this proposal and experiment E12-14-001 [9]. Measurement of the GDH integrand on the same nucleus used to study the polarized EMC effect will provide a "$Q^2 \to 0$ limit" of the latter. ^{7}Li has effective polarizations $P_A^p = 0.87$ and $P_A^n = -0.04$ from state-of-the-art quantum Monte Carlo calculations [49, 50]. The polarized proton is in the $1p_{3/2}$ shell which encounters lower density or has a greater spatial extent and will therefore experience less of the scalar and vector mean fields and may show smaller modification.

b. Carbon-13 ^{13}C has a single unpaired neutron. Dynamic nuclear polarization in this nuclear species has been studied extensively by the hyperpolarized MRI community [51], and the Bochum polarized target group has demonstrated 75% polarization of ^{13}C at 0.9 K and 5 T [52]. We anticipate similar or higher polarization at 0.3 K and 2.5 T.

c. Oxygen-17 ^{17}O has a single unpaired neutron outside the $Z = 8$ and $N = 8$ magic number closed shells and a reasonably large magnetic moment, making it a good candidate. Projections using EST for ^{17}O in butanol are very promising. However, as a spin-5/2 nucleus it will exhibit significant quadrupolar broadening in solid butanol, and accurate measurement of its NMR signal may be challenging.

A target made of water would dramatically increase the figure of merit due to a significantly smaller dilution but will require further development. The polarization of $H_2{}^{17}O$ by the hyperpolarized MRI community is in its naissance. However, the ^{17}O NMR signal has been enhanced by more than a factor of 100 at 5 T and 77 K in a eutectic mixture of gycerol and $H_2{}^{17}O$ [53].

d. Fluorine-19 As pointed out in [9], ^{11}B and ^{19}F are two nuclei where a single proton carries most of the nuclear spin. The valence proton in ^{19}F is in the $2s_{1/2}$ shell, an inner region far from the periphery, potentially making the data more easily interpretable. The magnetic moment is very close to that of the free proton. Large-scale shell model calculations [54] show that the neutron polarization in ^{19}F is very close to zero while the proton polarization is within $(5\pm0.6)\%$ of that of the whole nucleus. Targets could be made using irradiated ^{6}Li^{19}F where a high polarization of ^{19}F can reasonably be expected, based on the performance of

^{6}LiH. In the latter case, F-centers are produced in the crystal lattice using ionizing radiation, and these serve as the paramagnetic impurity for DNP. We anticipate similar behavior in lithium fluoride, which has identical structure.

Another option is ^{19}F in $C_3H_2F_6O$ which has a similar dilution factor and has been polarized to 80% [55] using the Cr(V) complex as the paramagnetic impurity.

3. *Exclusive Measurement*

For the exclusive measurement we will run long enough for a significant result on the single nucleus with the highest FOM. This is likely to ^{7}Li for the reasons described in Sec. V B 2 a—low dilution, high polarization and favorable nuclear physics. In addition, ^{7}Li is the subject of E12-14-001.

C. Uncertainties

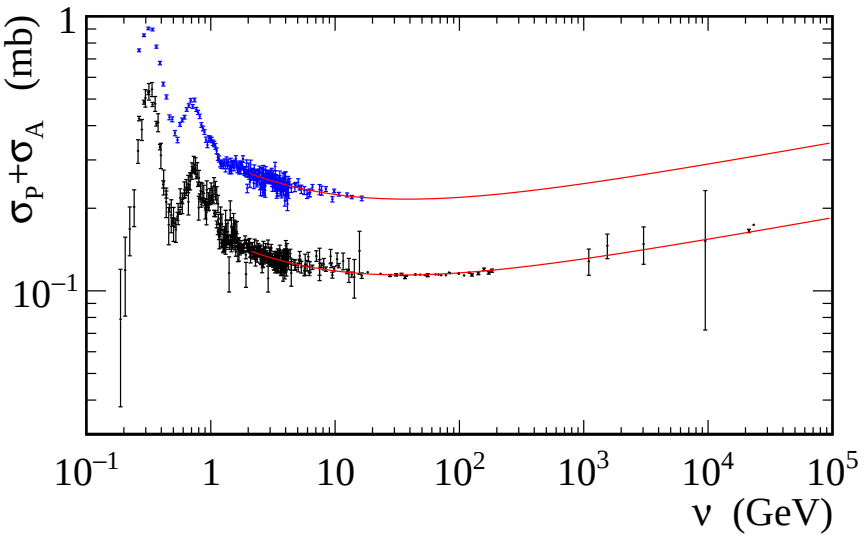

FIG. 6. Unpolarized total photoabsorption cross-section $\sigma_P + \sigma_A$ for the proton (black symbols) and deuteron (blue symbols) as a function of the photon beam energy. The data are from Ref. [56]. The lines are Regge fits including a pomeron term proportional to $\nu^{0.08}$.

The total photo nuclear cross section in the energy range $1 - 12\,\text{GeV}$ is $\approx 100\,\mu\text{b/A}$, Fig. 6. The helicity dependent cross section difference is expected to be $\approx -4\,\mu\text{b}$ for the proton and $\gtrapprox 7\,\mu\text{b}$ for the neutron, based on the existing Regge fits [1, 14]. This is an

inclusive photo-absorption asymmetry of 10^{-3} to 10^{-2} depening on the nucleus. Jefferson Lab has experience controlling beam related false asymmetries to extremely small levels for the parity violation program. Part per million control of the Hall D photon beam charge asymmetry would be achieved without a special effort [1]. The inclusive asymmetry is at least three orders of magnitude larger than the level where one should worry about beam false asymmetries.

D. Backgrounds

We are extracting a polarization observable so backgrounds with a polarization dependence are the main concern. Unpolarized backgrounds act only as dilution. For the GDH sum rule, which is a cross section difference rather that an asymmetry, unpolarized backgrounds cancel.

1. Coherent Nuclear Photoabsorption

Since the nucleus itself is polarized, coherent scattering off the whole nucleus may have a polarization dependent asymmetry which we must subtract to get the nucleon only contribution.

There is little existing data on coherent photoproduction from nuclei. The cross section for $\gamma\ ^3\mathrm{He} \to \eta\ ^3\mathrm{He}$ is $\approx 200\,\mathrm{nb}$ from threshold to 725 MeV [57–59] and for $\gamma\ ^7\mathrm{Li} \to \eta\ ^7\mathrm{Li}$ is $\sim 20\,\mathrm{nb}$ from threshold to 660 MeV [60], a full order of magnitude smaller. These values are small compared the total photo-absorption cross section ($\gtrapprox 3$ and $\gtrapprox 5$ orders of magnitude respectively) and small compared to the expected helicity dependent cross section difference from the nucleon, but are not measured in the energy range of interest here. The coherent cross section should decrease both with nuclear size and with photon energy making them even more manageable.

In terms of dealing with the coherent background, cross sections in the energy range of interest can be extracted from existing Hall D data on ^{2}H, ^{4}He and ^{12}C targets at high momentum transfer. Bounds on the helicity dependent cross section difference for coherent photoproduction should be obtainable directly for the nuclei of interest using exclusive analyses at high momentum transfer in this proposed data set.

The cross section for coherent π^0 production is large in the region of the $\Delta(1232)$ resonance [60]. While this is not a concern here, it might be for a sister experiment aiming to measure this contribution.

E. Beam Time Estimate

We will attempt to take equal statistical weight with each of the proposed inclusive targets. Achieving this depends primarily on accounting for the polarization that can be achieved for each target and the inherent dilution to the signal that comes from unpolarized nucleons in the target nucleus and in the other nuclei required for the target molecule. The experimental figure of merit is given by

$$f = P^2 F \,, \tag{13}$$

where P is the expected polarization and F is the dilution fraction.

Table II gives examples of nuclear species considered for use in this experiment and the hydrogen and deuterium targets for the approved experiment REGGE [1]. In particular we calculate the relative figure of merit for estimating the beam time requirements. Lower figure of merit will require more beam time to reach the same statistical precision. In order to estimate the rates we do a simple scaling from the very careful estimates done in Ref. [1]. We attempt to give each nuclear target about ½ the statistics that were approved for the hydrogen and deuterium run. We use conservative estimates of the expected polarization. The final choice of nuclei and molecule will depend on the results achieved during target development. For example, a butanol target with ^{17}O polarized to 80% has the same figure of merit as a water target with ^{17}O polarized to 40%.

At each beam energy, we expect an overhead of about 1 day per target to swap materials, repolarize and commission, and 2 days of systematic studies. This leads to a total of about 7 PAC weeks at 12 GeV and 4 PAC weeks at 4 GeV for the inclusive measurement. As described in Sec. IV, 4 PAC weeks of running at 12 GeV should be sufficient to observe a diluted asymmetry to 5σ. Considering that a week of running on ^{7}Li was included in the 7 weeks for inclusive measurement, this gives a total of 10 weeks at 12 GeV. Sec. IV also discussed a scenario in which an additional 12 weeks are used to map out the dependence of

the asymmetry on $k_{\rm miss}$. We would appreciate guidance on whether such an extension might be considered favorably.

VI. CONCLUSION

We present ideas to measure the helicity dependent photo-absorption cross section $\Delta\sigma$ on a polarized nucleon in various nuclei. We use the power of the GDH sum rule to argue that there must be significant modification of $\Delta\sigma$ in the energy range of this measurement. This will allow the study of the modification of the Regge parameters α_{f1} and α_{a1} in the nuclear medium to high precision. In addition we will test whether two nucleons in a Short Range Correlation become depolarized by directly measuring various target asymmetries for correlated pair both in and outside of SRCs.

After the accepted Jefferson Lab experiment E12-14-001 [9], focusing on polarized DIS, viz $Q^2 > 1\,\mathrm{GeV}^2$, these are the only measurements using polarization observables to study medium modifications that we are aware of. Given that a significant fraction of that data will be taken on ^{7}Li, the same nucleus as E12-14-001, these data is directly complementary to those of E12-14-001 and will significantly improve on the total polarized data set available for ^{7}Li. In addition, it will introduce 3 other new polarized species to the world data, allowing for the dependence on of medium modifications on parameters such as isospin, virtuality or local density to be investigated.

Inclusive measurements have a major statistical advantage over exclusive measurements and are often the first to be carried out on any system. This proposal exploits this to obtain compelling data on a number of different nuclei. The use of a photon beam in the Hall D setup is very advantageous for polarized nuclear targets and allows targets that are not practical with an electron beam because the polarization would be too low.

We intend to begin a research project with the Jefferson Lab target group to investigate which nuclear species and substances can be made to have the highest FOM as a nuclear physics target. We would like to motivate theoretical support for calculations in the energy range of this proposal, for example of the asymmetry $\mathbb{E}$ for various final states, the total coherent nuclear photo-absorption cross section, and the helicity dependent total coherent nuclear photo-absorption cross section. While the data from this experiment alone are compelling and interesting, completing the GDH sum rule will complete the interpretation

as a modification of κ. This will require additional data from pion production threshold to $\sim 1.5\,\mathrm{GeV}$, a range that could be covered at Bonn with their existing polarized target apparatus.

VII. ACKNOWLEDGEMENTS

We acknowledge helpful conversations with Steven Bass and Ian Cloet.

VIII. APPENDIX: TABLE OF NUCLEI

Stable nuclei with a known magnetic moment. The anomalous magnetic moment is calculated from Eqn. (6) and the GDH sum from Eqn. (2). Data are from the IAEA [61] and may contain omissions (^{19}F was added by hand).

TABLE III: Stable nuclei with a known magnetic moment.

	$J\pi$	μ	κ	M	I_{GDH}
^{1}H	1/2+	2.793	1.793	0.9383	204.8
^{2}H	1+	0.857	-0.1426	1.875	0.6484
^{3}He	1/2+	-2.128	-8.383	2.808	499.9
^{6}Li	1+	0.822	-0.5338	5.600	1.019
^{7}Li	3/2−	3.256	4.598	6.532	83.39
^{9}Be	3/2−	-1.178	-7.533	8.390	135.7
^{10}B	3+	1.801	-1.999	9.322	15.47
^{11}B	3/2−	2.689	4.858	10.25	37.81
^{13}C	1/2−	0.702	3.131	12.11	3.753
^{14}N	1+	0.404	-4.174	13.04	11.50
^{15}N	1/2−	-0.283	-11.25	13.96	36.39
^{17}O	5/2+	-1.894	-14.44	15.83	233.4
^{19}F	1/2+	2.628	40.94	17.69	300.5
^{21}Ne	3/2+	-0.662	-14.63	19.55	94.31
^{23}Na	3/2+	2.217	6.001	21.40	13.23
^{25}Mg	5/2+	-0.855	-16.28	23.26	137.3
^{27}Al	5/2+	3.642	6.664	25.12	19.74
^{29}Si	1/2+	-0.555	-30.10	26.98	69.84
^{31}P	1/2+	1.131	20.06	28.84	27.14
^{33}S	3/2+	0.644	-8.918	30.70	14.20
^{35}Cl	3/2+	0.822	-7.411	32.56	8.721
^{37}Cl	3/2+	0.684	-8.562	34.41	10.42
^{39}K	3/2+	0.391	-13.91	36.27	24.75
^{41}K	3/2+	0.215	-16.06	38.13	29.86
^{43}Ca	7/2−	-1.317	-28.09	39.99	193.7
^{45}Sc	7/2−	4.756	9.577	41.85	20.56
^{47}Ti	5/2−	-1.100	-32.34	43.71	153.5
^{49}Ti	7/2−	-1.104	-29.73	45.57	167.1
^{53}Cr	3/2−	-0.475	-32.38	49.29	72.64
^{55}Mn	5/2−	3.453	12.99	51.15	18.08
^{57}Fe	1/2−	0.090	-20.84	53.01	8.674
^{59}Co	7/2−	4.627	12.00	54.87	18.78
^{61}Ni	3/2−	-0.750	-43.25	56.73	97.81
^{63}Cu	3/2−	2.223	17.69	58.59	15.34
^{65}Cu	3/2−	2.382	22.60	60.45	23.52
^{67}Zn	5/2−	0.875	-18.27	62.31	24.11
^{69}Ga	3/2−	2.017	15.38	64.17	9.668
^{71}Ga	3/2−	2.562	29.64	66.03	33.91
^{73}Ge	9/2+	-0.879	-39.13	67.89	167.7
^{75}As	3/2−	1.439	2.987	69.75	0.3085
^{77}Se	1/2−	0.534	7.084	71.61	0.5489
^{79}Br	3/2−	2.106	20.47	73.47	13.06
^{81}Br	3/2−	0.129	-31.52	75.33	29.45
^{83}Kr	9/2+	-0.971	-44.95	77.19	171.2
^{85}Rb	5/2−	1.353	-14.00	79.05	8.795
^{87}Sr	9/2+	-1.093	-48.56	80.91	181.9
^{89}Y	1/2−	-0.137	-51.23	82.77	21.49
^{91}Zr	5/2+	-1.304	-63.73	84.63	159.0
^{93}Nb	9/2+	6.170	22.76	86.49	34.96
^{95}Mo	5/2+	-0.914	-59.37	88.36	126.6
^{97}Mo	5/2+	-0.933	-60.11	90.22	124.5
^{99}Ru	5/2+	-0.641	-56.69	92.08	106.3
^{101}Ru	5/2+	-0.719	-58.52	93.94	108.8

Continued on next page

TABLE III – from previous page

	$J\pi$	μ	κ	M	$I_{\rm GDH}$
^{103}Rh	1/2−	-0.088	-54.11	95.80	17.89
^{105}Pd	5/2+	-0.642	-59.48	97.67	104.0
^{107}Ag	1/2−	-0.114	-59.15	99.53	19.81
^{109}Ag	1/2−	-0.131	-61.25	101.4	20.47
^{111}Cd	1/2+	-0.595	-114.0	103.3	68.41
^{115}Sn	1/2+	-0.919	-155.7	107.0	118.8
^{117}Sn	1/2+	-1.001	-167.1	108.8	132.2
^{119}Sn	1/2+	-1.047	-174.6	110.7	139.6
^{121}Sb	5/2+	3.363	30.39	112.6	20.45
^{123}Sb	7/2+	2.550	-6.196	114.4	1.151
^{125}Te	1/2+	-0.889	-163.1	116.3	110.3
^{127}I	5/2+	2.813	18.46	118.1	6.844
^{129}Xe	1/2+	-0.778	-154.4	120.0	92.79
^{131}Xe	3/2+	0.692	-23.79	121.9	6.411
^{133}Cs	7/2+	2.582	-5.942	123.7	0.9053
^{135}Ba	3/2+	0.838	-18.29	125.6	3.569
^{137}Ba	3/2+	0.936	-13.26	127.5	1.822
^{139}La	7/2+	2.783	-1.737	129.3	0.07081
^{141}Pr	5/2+	4.275	61.57	131.2	61.77
^{143}Nd	7/2−	-1.065	-81.76	133.0	148.3
^{145}Nd	7/2−	-0.656	-73.59	134.9	116.8
^{149}Sm	7/2−	-0.668	-76.21	138.6	118.6
^{153}Eu	5/2+	1.532	-16.11	142.4	3.590
^{155}Gd	3/2−	-0.257	-77.30	144.2	48.33
^{157}Gd	3/2−	-0.340	-81.78	146.1	52.73
^{159}Tb	3/2+	2.014	41.74	148.0	13.39
^{161}Dy	5/2+	-0.480	-81.47	149.8	82.92
^{163}Dy	5/2−	0.673	-44.07	151.7	23.68
^{165}Ho	7/2−	4.177	31.46	153.5	16.48
^{167}Er	7/2+	-0.564	-81.45	155.4	107.8
^{169}Tm	1/2+	-0.232	-108.1	157.3	26.52
^{171}Yb	1/2−	0.494	14.42	159.1	0.4604
^{173}Yb	5/2−	-0.680	-93.52	161.0	94.63
^{175}Lu	7/2+	2.233	-15.18	162.9	3.412
^{177}Hf	7/2−	0.793	-51.94	164.7	39.03
^{179}Hf	9/2+	-0.641	-84.75	166.6	130.6
^{181}Ta	7/2+	2.370	-11.71	168.5	1.896
^{185}Re	5/2+	3.187	42.92	172.2	17.43
^{187}Os	1/2−	0.065	-63.91	174.1	7.562
^{189}Os	3/2−	0.660	-34.42	175.9	6.443
^{191}Ir	3/2+	0.151	-67.41	177.8	24.19
^{193}Ir	3/2+	0.164	-66.47	179.6	23.03
^{195}Pt	1/2−	0.610	40.86	181.5	2.842
^{199}Hg	1/2−	0.506	20.67	185.2	0.6985
^{201}Hg	3/2−	-0.560	-117.5	187.1	66.40
^{203}Tl	1/2+	1.616	247.0	189.0	95.87
^{205}Tl	1/2+	1.638	254.8	190.8	100.0

[1] M. M. Dalton, A. Deur, C. D. Keith, S. Širca, and J. Stevens, (2020), arXiv:2008.11059 [nucl-ex].

[2] J. J. Aubert et al. (European Muon), Phys. Lett. B **123**, 275 (1983).

[3] A. W. Thomas, A. Michels, A. W. Schreiber, and P. A. M. Guichon, Phys. Lett. B **233**, 43 (1989).

[4] L. L. Frankfurt and M. I. Strikman, Phys. Rept. **160**, 235 (1988).

[5] O. Hen, D. W. Higinbotham, G. A. Miller, E. Piasetzky, and L. B. Weinstein, Int. J. Mod. Phys. E **22**, 1330017 (2013), arXiv:1304.2813 [nucl-th].

[6] J. Arrington et al., Prog. Part. Nucl. Phys. **127**, 103985 (2022), arXiv:2112.00060 [nucl-ex].

[7] B. S. Pudliner, V. R. Pandharipande, J. Carlson, and R. B. Wiringa, Phys. Rev. Lett. **74**, 4396 (1995), arXiv:nucl-th/9502031.

[8] A. W. Thomas, Int. J. Mod. Phys. E **27**, 1840001 (2019), arXiv:1809.06622 [hep-ph].

[9] S. Kuhn and W. Brooks, "The EMC Effect in Spin Structure Functions," Proposal to Jefferson Lab PAC (2014).

[10] I. C. Cloet, W. Bentz, and A. W. Thomas, Phys. Rev. Lett. **109**, 182301 (2012), arXiv:1202.6401 [nucl-th].

[11] O. Hen, G. A. Miller, E. Piasetzky, and L. B. Weinstein, Rev. Mod. Phys. **89**, 045002 (2017), arXiv:1611.09748 [nucl-ex].

[12] S. B. Gerasimov, Sov. J. Nucl. Phys. **2**, 430 (1966).

[13] D. Drechsel and L. Tiator, Ann. Rev. Nucl. Part. Sci. **54**, 69 (2004), arXiv:nucl-th/0406059.

[14] K. Helbing, Prog. Part. Nucl. Phys. **57**, 405 (2006), arXiv:nucl-ex/0603021.

[15] D. Drechsel and T. Walcher, Rev. Mod. Phys. **80**, 731 (2008), arXiv:0711.3396 [hep-ph].

[16] X. Zheng et al. (CLAS), Nature Phys. **17**, 736 (2021), arXiv:2102.02658 [nucl-ex].

[17] V. Sulkosky et al. (E97-110), Phys. Lett. B **805**, 135428 (2020), arXiv:1908.05709 [nucl-ex].

[18] V. A. Sulkosky, The spin structure of ^{3}He and the neutron at low Q^2: A measurement of the generalized GD Ph.D. thesis, William-Mary Coll. (2007).

[19] L. Morejon, A. Fedynitch, D. Boncioli, D. Biehl, and W. Winter, JCAP **11**, 007 (2019), arXiv:1904.07999 [astro-ph.HE].

[20] M. Broz, J. G. Contreras, and J. D. Tapia Takaki, Comput. Phys. Commun. **253**, 107181

(2020), arXiv:1908.08263 [nucl-th].

[21] S. D. Bass, Acta Phys. Polon. B **52**, 43 (2021), arXiv:2006.10601 [hep-ph].

[22] S. D. Bass, P. Pedroni, and A. Thomas, (2022), arXiv:2212.04795 [nucl-th].

[23] K. Saito, K. Tsushima, and A. W. Thomas, Prog. Part. Nucl. Phys. **58**, 1 (2007), arXiv:hep-ph/0506314.

[24] K. Saito and A. W. Thomas, Phys. Rev. C **51**, 2757 (1995), arXiv:nucl-th/9410031.

[25] A. S. Carroll, I. H. Chiang, C. B. Dover, T. F. Kycia, K. K. Li, P. O. Mazur, D. N. Michael, P. M. Mockett, D. C. Rahm, and R. Rubinstein, Phys. Rev. C **14**, 635 (1976).

[26] B. Krusche, J. Ahrens, R. Beck, I. J. D. MacGregor, J. C. McGeorge, V. Metag, and H. Stroher, Phys. Rev. Lett. **86**, 4764 (2001), arXiv:nucl-ex/0304010.

[27] S. D. Bass and A. W. Thomas, Phys. Lett. B **634**, 368 (2006), arXiv:hep-ph/0507024.

[28] R. Averbeck, in 4th TAPS International Workshop on Electromagnetic and Hadronic Probes of Nuclear Mat (1998) arXiv:nucl-ex/9803001.

[29] M. Röbig-Landau et al., Phys. Lett. B **373**, 45 (1996).

[30] T. Yorita et al., Phys. Lett. B **476**, 226 (2000).

[31] T. Mertens et al. (CBELSA, TAPS), Eur. Phys. J. A **38**, 195 (2008), arXiv:0810.2678 [nucl-ex].

[32] B. Krusche and C. Wilkin, Prog. Part. Nucl. Phys. **80**, 43 (2015), arXiv:1410.7680 [nucl-ex].

[33] I. Strakovsky, S. Širca, W. J. Briscoe, A. Deur, A. Schmidt, and R. L. Workman, Phys. Rev. C **105**, 045202 (2022), arXiv:2201.06495 [nucl-th].

[34] S. D. Bass and M. M. Brisudova, Eur. Phys. J. A **4**, 251 (1999), arXiv:hep-ph/9711423.

[35] S. Tronchin, H. H. Matevosyan, and A. W. Thomas, Phys. Lett. B **783**, 247 (2018), arXiv:1806.00481 [nucl-th].

[36] I. C. Cloet, W. Bentz, and A. W. Thomas, Phys. Rev. Lett. **95**, 052302 (2005), arXiv:nucl-th/0504019.

[37] I. Cloet, W. Bentz, and A. W. Thomas, Phys. Lett. B **642**, 210 (2006), arXiv:nucl-th/0605061.

[38] I. Senderovich et al. (CLAS), Phys. Lett. B **755**, 64 (2016), arXiv:1507.00325 [nucl-ex].

[39] Z. Akbar et al. (CLAS), Phys. Rev. C **96**, 065209 (2017), arXiv:1708.02608 [nucl-ex].

[40] M. Gottschall et al. (CBELSA/TAPS), Eur. Phys. J. A **57**, 40 (2021), arXiv:1904.12560 [nucl-ex].

[41] K. Chan et al., (2023), arXiv:2305.08616 [nucl-ex].

[42] P. Solvignon et al. (Jefferson Lab E01-012), Phys. Rev. Lett. **101**, 182502 (2008),

arXiv:0803.3845 [nucl-ex].

[43] V. Lagerquist, S. E. Kuhn, and N. Sato, Phys. Rev. C **107**, 045201 (2023), arXiv:2205.01218 [nucl-ex].

[44] Hen O. and others, "Studying Short-Range Correlations with Real Photon Beams at GlueX," (2019).

[45] P. Navrátil, S. Quaglioni, G. Hupin, C. Romero-Redondo, and A. Calci, Phys. Scripta **91**, 053002 (2016), arXiv:1601.03765 [nucl-th].

[46] J. Arrington, A. Daniel, and D. Gaskell, "The EMC Effect in Spin Structure Functions," Proposal to Jefferson Lab PAC (2010).

[47] J. Ball et al., Nucl. Instrum. Meth. A **498**, 101 (2003).

[48] K. Kondo et al., Nucl. Instrum. Meth. A **526**, 70 (2004).

[49] B. S. Pudliner, V. R. Pandharipande, J. Carlson, S. C. Pieper, and R. B. Wiringa, Phys. Rev. C **56**, 1720 (1997), arXiv:nucl-th/9705009.

[50] R. B. Wiringa, R. Schiavilla, S. C. Pieper, and J. Carlson, Phys. Rev. C **89**, 024305 (2014), arXiv:1309.3794 [nucl-th].

[51] Z. J. Wang et al., Radiology **291**, 273 (2019).

[52] W. Meyer, J. Heckmann, C. Hess, E. Radtke, G. Reicherz, L. Triebwasser, and L. Wang, Nucl. Instrum. Meth. A **631**, 1 (2011).

[53] V. K. Michaelis, B. Corzilius, A. A. Smith, , and R. G. Griffin, J. Phys. Chem. B **117**, 14894–14906 (2013).

[54] P. Klos, J. Menéndez, D. Gazit, and A. Schwenk, Phys. Rev. D **88**, 083516 (2013), [Erratum: Phys.Rev.D 89, 029901 (2014)], arXiv:1304.7684 [nucl-th].

[55] D. Hill, T. Kasprzyk, J. J. Jarmer, S. Penttila, M. Krumpolc, G. W. Hoffmann, and M. Purcell, Nucl. Instrum. Meth. A **277**, 319 (1989).

[56] M. Tanabashi et al. (Particle Data Group), Phys. Rev. D **98**, 030001 (2018).

[57] M. Pfeiffer et al., Phys. Rev. Lett. **92**, 252001 (2004), arXiv:nucl-ex/0312011.

[58] M. Pfeiffer et al., Phys. Rev. Lett. **94**, 049102 (2005).

[59] F. Pheron et al., Phys. Lett. B **709**, 21 (2012), arXiv:1201.6517 [nucl-ex].

[60] Y. Maghrbi et al. (Crystal Ball), Eur. Phys. J. A **49**, 38 (2013), arXiv:1303.2254 [nucl-ex].

[61] International Atomic Energy Agency, "IAEA Nuclear Data Services," (2023), [Online; accessed 10-March-2023].